HHS Public Access

Author manuscript

Biomaterials. Author manuscript; available in PMC 2018 January 01.

Published in final edited form as:

Biomaterials. 2017 January ; 112: 303–312. doi:10.1016/j.biomaterials.2016.10.013.

POLYMER FIBER-BASED MODELS OF CONNECTIVE TISSUE REPAIR AND HEALING

Nancy M. Lee[1], **Cevat Erisken**[1], **Thomas Iskratsch**[2], **Michael Sheetz**[2], **William N. Levine**[3], and **Helen H. Lu**[1,4]

[1] Biomaterials and Interface Tissue Engineering Laboratory, Department of Biomedical Engineering, Columbia University, New York, NY 10027

[2] Department of Biological Sciences, Columbia University, 713 Fairchild Center, MC 2408, New York, NY 10027

[3] Department of Orthopaedic Surgery, Columbia University Medical Center, New York, NY 10032

Abstract

Physiologically relevant models of wound healing are essential for understanding the biology of connective tissue repair and healing. They can also be used to identify key cellular processes and matrix characteristics essential for the design of soft tissue grafts. Modeling the various stages of repair post tendon injury, polymer meshes of varying fiber diameter (nano-1 (390 nm) < nano-2 (740 nm) < micro (1420 nm)) were produced. Alignment was also introduced in the nano-2 group to model matrix undergoing biological healing rather than scar formation. The response of human tendon fibroblasts on these model substrates were evaluated over time as a function of fiber diameter and alignment. It was observed that the repair models of unaligned nanoscale fibers enhanced cell growth and collagen synthesis, while these outcomes were significantly reduced in the mature repair model consisting of unaligned micron-sized fibers. Organization of paxillin and actin on unaligned meshes was enhanced on micro-compared to nano-sized fibers, while the expression and activity of RhoA and Rac1 were greater on nanofibers. In contrast, aligned nanofibers promoted early cell organization, while reducing excessive cell growth and collagen production in the long term. These results show that the early-stage repair model of unaligned nanoscale fibers elicits a response characteristic of the proliferative phase of wound repair, while the more mature model consisting of unaligned micron-sized fibers is more representative of the remodeling phase by supporting cell organization while suppressing growth and biosynthesis. Interestingly, introduction of fiber alignment in the nanofiber model alters fibroblast response from repair to healing, implicating matrix alignment as a critical design factor for circumventing scar formation and promoting biological healing of soft tissue injuries.

[4]To whom all correspondence should be addressed: Helen H. Lu, Ph.D., Department of Biomedical Engineering, Columbia University, 351 Engineering Terrace Building, MC 8904, 1210 Amsterdam Avenue, New York, NY 10027, 212-854-4071 (office); 212-854-8725 (fax), hhlu@columbia.edu.

All authors have no conflicts of interest

Keywords

wound repair model; fiber diameter; alignment; tendon

Introduction

The repair of injured connective tissues such as ligaments or tendons begins with an inflammatory response followed by a proliferative phase, in which the predominate cell types are fibroblasts, macrophages, and mast cells. A disorganized collagen fiber matrix is first laid down[1], and the collagen fibers deposited during this period display a fiber diameter smaller than that of native tissue[2,3] (Figure 1: Stage 1 and 2). The next phase of wound repair is the remodeling phase, which is characterized by both increasing collagen fiber diameter and organization (Figure 1: Stage 3 and Repair), augmenting the tensile strength of the repairing tissue[3,4]. As a consequence of how both collagen fiber diameter and organization during wound repair deviate from those of the healthy extracellular matrix (ECM), regeneration or true biological healing is not achieved and the repaired tissue is often compositionally and mechanically inferior to native matrix[1,5,6]. This results in suboptimal performance of the repaired tissue[7] and increases the potential for reinjury. The disparity that exists between normal and scar/repaired tissue underscores the need for physiologically relevant matrix models, which can be used to investigate the cellular and matrix processes that differ between wound repair and biological healing. Such models will also be critical for the design of functional grafts to enhance connective tissue regeneration.

It has been reported that the response of a variety of cell types including fibroblasts[8-10], osteoblasts[11] and mesenchymal stem cells (MSCs)[12,13] can be modulated by the underlying substrate topography, namely fiber diameter and alignment. Specifically, fibroblast organization[8], matrix production[9], and migration[10] were enhanced by culture on aligned compared to unaligned nanofiber matrices. Investigating the effects of fiber diameter using unaligned polylactide-*co*-glycolide (PLGA) fibers, Bashur *et al.* observed diminished spreading and lower aspect ratio for NIH 3T3 mouse fibroblasts cultured on 140 nm and 760 nm fibers compared to 3.6 μm fibers[14]. Stem cells grown on unaligned polyurethane meshes measured greater cell density on submicron (0.28, 0.82 μm) meshes compared to 2.3 μm fibers[15]. More recently, Erisken *et al.* observed a diameter-dependent response on tendon fibroblasts cultured on aligned PLGA meshes, whereby nanofibers regulated cell proliferation and production, while the microfibers upregulated the expression of fibroblastic markers[16].

These findings underscore the complex relationship between the sub-cellular geometry and global cell function. Cells respond to their 3D environment through cytoskeletal actin stress fibers[17] and focal adhesions which activate downstream signaling pathways[18]. This outside-in signaling is known to affect critical cell functions including adhesion, migration, morphology, proliferation, gene expression, and differentiation[18-22]. Accordingly, interactions between cells and their local environment play a significant role in both tissue homeostasis and wound repair[23]. As wounds are heterogeneous and dynamic, the repair process is complex and influenced by factors such as extracellular matrix components and

growth factors[24,25], that can lead to scar tissue formation instead of tissue regeneration or biological healing. Model systems that recapitulate the dynamic characteristic of the extracellular matrix during repair or healing can be used to investigate the biological mechanisms guiding these distinct processes. Such *in vitro* wound repair models will allow for the controlled examination of the tissue response to the environmental factor or change, isolating the effects from other cells or tissues inherent in *in vivo* models[26]. Furthermore, comparisons between models of tissue repair for which the outcome is scar tissue, and models of tissue regeneration or biological healing, which results in recapitulation of native tissue architecture and function, will be instrumental to the design of biomaterials and grafts that will promote tissue regeneration.

To this end, the focus of this study is to develop polymer fiber-based models of tendon repair and healing and to examine the response of human tendon fibroblasts to these substrates. Specifically in this work, tissue repair refers to the events characteristic of the formation of scar or physiologically inferior tissue, while healing or regeneration refers to the restoration of native tissue properties. Given that collagen fiber diameter increases during tissue healing[2-4], it is hypothesized that nanometer diameter fibers will promote cell proliferation and matrix deposition, similar to the proliferative phase of wound repair, modeled by Stages 1 and 2 in Figure 1. This is in comparison to the more mature stage of repair, as represented by Stage 3. Furthermore, as it is established that collagen fibers become more aligned from an initial unorganized tissue during wound repair[3,4], cell response elicited by nanofiber organization is also examined here. By keeping fiber diameter constant, these groups will allow for the decoupling of effects based on fiber alignment and diameter. It is anticipated that cell attachment and spreading, as well as the expression of fibroblastic markers will be promoted on aligned fibers, while unaligned fibers will enhance proliferation and matrix deposition. The elucidation of these wound repair and regeneration interactions is anticipated to reveal parameters critical to the design of functional scaffolds that will promote biological healing instead of scar tissue formation post injury.

Materials and Methods

Mesh Fabrication and Characterization

Unaligned polylactic-*co*-glycolic acid (PLGA) meshes of three fiber diameter ranges were fabricated by electrospinning[25;26] according to conditions outlined in Table 1. Briefly, granules of PLGA (85:15, DL, $M_w \approx 123.6$ kDa, Lakshore Biomaterials, Birmingham, AL) were premixed in a solution of acetone (Ace, Sigma-Aldrich, St. Louis, MO) and N,N-dimethylformamide (DMF, Sigma-Aldrich), followed by the addition of 14% v/v ethanol (Decon, King of Prussia, PA). The polymer solution (32%, 43% and 50% w/v) was loaded into a 5-mL syringe attached with a blunt-tip needle, and dispensed using a syringe pump (Harvard Apparatus, Holliston, MA). A voltage of 8-10 kV was applied to the needle, and fibers were collected on a grounded stationary plate placed at a distance of 13-15 cm from the needle tip. To fabricate aligned nanofibers, PLGA was premixed with DMF, followed by the addition of 0.5 mL ethanol, yielding a 54% w/v solution. The polymer solution was loaded into a 5-mL syringe with an 18.5 gauge blunt-tip needle, and electrospun at a voltage of 8-10 kV and a flow rate of 1 mL/hr. Fibers were collected on a grounded rotating mandrel

(2500 rpm) placed at a 12 cm distance from the needle tip. All polymer solutions were electrospun to achieve a thickness of 0.10 ± 0.02 mm.

The fiber diameter, alignment, and morphology of as-fabricated matrices were analyzed by scanning electron microscopy (SEM, 1-2.5 kV, 10 μA Hitachi 4700, Tokyo, Japan). Prior to SEM imaging, samples were coated (Cressington 108auto, Watford, England) with a layer of gold-palladium **(10 seconds, 2 nm)**. Fiber diameter, measured using ImageJ (National Institutes of Health, Bethesda MD), is reported as an average of measurements taken from three independent regions (n=6 images/group), with 20 measurements (10-15 fibers) per image. Fiber alignment (n=6) was quantified using the method of Costa *et al.*[27], in which SEM images were analyzed using circular statistics software customized for evaluating fiber alignment (Fiber3). Parameters include: (1) the mean vector angle (MA), which represents the average fiber alignment in the matrix ($|\theta| \leq 90°$), with 0° representing a horizontal orientatio n; (2) the mean vector length (MVL, $0 \leq r \leq 1$), in which 0 indicates a random and 1 an aligned morphology; and (3) angular deviation (AD) which characterizes the dispersion of the non-Gaussian angle distribution of the nanofibers ($0° \leq \theta \leq 40.5°$), whereby 0° represents aligned and 40.5° a random distribution.

Cells and Cell Culture

Human rotator cuff fibroblasts were isolated from explant culture of tissues obtained from patients (male aged 51- 65 years, female 76 years, institutional review board exempt) who underwent rotator cuff repair surgery. Briefly, tissue samples were rinsed with phosphate buffered saline (PBS, Sigma-Aldrich), plated in tissue culture dishes, and maintained in Dulbecco's modified Eagle medium (DMEM) supplemented with 10% fetal bovine serum (FBS, Atlanta Biologicals, Lawrenceville, GA), 1% non-essential amino acids, 1% penicillin/streptomycin, 0.1% amphotericin B and 0.1% gentamicin/sulfate (fully supplemented media). The cells from the first and second migrations were discarded, and the tissue was re-plated in fresh media. Only cells obtained from the third migration were used in this study as this method has been shown to yield a relatively homogenous fibroblast population[28]. Prior to seeding, cells from all donors were pooled. All media and supplements were purchased from Mediatech (Herndon, VA) unless otherwise noted.

Cell Seeding on Scaffolds

Prior to seeding, the polymer scaffolds were secured using custom-made clamps, sterilized with UV radiation (356nm), and preincubated (37°C, 5% CO_2) in DMEM supplemented with 20% FBS overnight to promote cell attachment. Fibroblasts (passage 4-5) were seeded at density of 30,000 cells/cm^2, and were cultured for up to four weeks in fully supplemented DMEM containing 50 μg/mL ascorbic acid[29] (Sigma-Aldrich). Cells were maintained at 37°C, 5% CO_2 and media was exchanged every 2-3 days. The effect of fiber diameter and alignment on cell morphology, attachment, proliferation, gene expression and matrix production were determined over four weeks of culture.

Cell Viability and Adhesion

Cell viability (n=3) was visualized using Live/Dead staining (Molecular Probes, Eugene, OR) following the manufacturer's protocol. Samples were imaged using confocal

microscopy (Olympus Fluoview FV100, Center Valley, PA) at excitation wavelengths of 488 nm and 568 nm. For alignment analysis, cell viability images (n=3, two regions/sample) were evaluated using circular statistics software, as described in the procedure for evaluating fiber alignment.

Immunohistochemistry (n=3) was performed to visualize paxillin focal adhesions and the actin cytoskeleton. Briefly, samples were rinsed in PBS, fixed for 10 minutes at room temperature in a 4% paraformaldehyde solution (pH 7.2), followed by a 10 minute permeabilization in 0.1% Triton-X (Sigma-Aldrich). Blocking was performed by immersion in a 1% BSA and 5% goat serum (Jackson Laboratories, Bar Harbor, ME) in immunostaining buffer solution (20mM TRIS, 155mM NaCl, 2nM EGTA, 2mM $MgCl_2$, pH 7.4) for 1 hour. Samples were incubated with paxillin primary antibody (1:500 dilution, BD Biosciences, Franklin Lakes, NJ) for 1 hour at room temperature, and then with secondary antibody (Alexa Fluor 555, 1:300 dilution, Invitrogen), along with Alexa Fluor 647 conjugated phallodin (1:100 dilution, Invitrogen) for 1 hour at room temperature. The samples were subsequently incubated with DAPI nuclear counterstain for 30 minutes, then mounted and imaged with confocal microscopy. All antibody dilutions were performed in immunostaining buffer containing 1% BSA.

Quantitative analysis of Rac1 activation (n=6) was performed using the G-LISA Rac activation assay (Cytoskeleton, Denver CO), according to the manufacturer's specifications. Briefly, after one day of culture scaffolds were rinsed with PBS and 100μl of lysis buffer was added to the samples. The lysates were collected, snap frozen, and stored at −80°C until analysis. Rac activity was d etermined using a 1:250 dilution of the primary antibody and 1:200 dilution of the secondary antibody. Horseradish peroxidase reagent was used to detect samples and luminescence was quantified (Tecan, Research Triangle Park, NC) using an integration time of 10 ms and gain of 100. Results were normalized to the total cell number.

Cell Proliferation

Total DNA content (n=5) was measured using the PicoGreen double stranded DNA assay (Invitrogen, Carlsbad, CA). At each time point, the samples were homogenized in 0.1% Triton-X and subjected to ultrsonication at 5W (Microson XL-2000, Qsonica, Newton, CT) for 15 seconds. Fluorescence was measured with a Tecan microplate reader at excitation and emission wavelengths of 485 and 535 nm respectively. Cell number was determined using a conversion factor of 8pg DNA/cell[30].

Cell Matrix Production

Collagen production (n=5) was quantified with a modified hydroxyproline assay[30]. Briefly, the samples were first desiccated (CentriVap, Labconco, Kansas City, MO) and digested for 18 hours at 65°C in a solution of 20 μL/mL papain (Sigma-Aldrich), buffered in 0.1 M sodium acetate, 10 mM cysteine HCl, and 50 M ethylenediaminetetraacetate. A 250 μl aliquot of the digest was concentrated by desiccation and samples were subsequently hydrolyzed in 10μl of 10N NaOH and autoclaved for 25 min. The hydrolysate was then oxidized by a buffered chloramine-T reagent for 25 min before the addition of Ehrlich's reagent. Sample absorbance was measured at 550 nm (Tecan), and collagen content was

obtained by interpolation along a standard curve generated using bovine collagen I (Sigma-Aldrich).

Matrix and cell distribution (n=2) was also visualized using hematoxylin and eosin (H&E, Sigma-Aldrich) and Picrosirius red stains[31]. Briefly, samples were fixed overnight in a 10% neutral buffered formalin containing 1% cetylpyridinium chloride (Sigma-Aldrich) solution, and subsequently stored in 0.01 M cacodylic acid (Sigma-Aldrich) until sectioning. Scaffolds were embedded in 5% poly vinyl alcohol (Sigma-Aldrich) frozen sectioning medium, and cut in cross-section to 10 μm thickness using a cryostat (Bright Instrument Company, Cambridgeshire, England).

Gene Expression

The expression of the fibroblastic markers type I and III collagen, intergrins α2 and β1, and the Rho GTPases RhoA, Rac1, and Cdc42 were measured at days 7 and 14 using quantitative reverse transcriptase-polymerase chain reaction (qRT-PCR, n=5), with custom-design primers (Table 2). Total RNA was isolated via Trizol extraction (Invitrogen), and then reverse-transcribed into cDNA using the SuperScript III First-Strand Synthesis System (Invitrogen). The cDNA product was amplified and quantified through real-time PCR using SYBR Green Supermix (Invitrogen). Glyceraldehyde-3-phosphate dehydrogenase (GAPDH) served as the house-keeping gene. All reactions were run for 50 cycles using the iCycler iQ Real-Time PCR Detection System (BioRad, Hercules, CA). Normalized expression levels were calculated based on the difference between threshold cycles of the gene of interest and GAPDH.

Statistical Analyses

Results are reported as mean ± standard deviation, with n equal to the number of replicates per group. One-way analysis of variance (ANOVA) was performed to determine the effects of fiber diameter or organization on scaffold structural and mechanical properties. Two-way ANOVA was used to determine fiber diameter and/or organization and temporal effects on cell proliferation, matrix production and gene expression. The Tukey-Kramer *post hoc* test was used for all pair-wise comparisons, and significance was attained at $p < 0.05$. Statistical analyses were performed with JMPIN (4.0.4, SAS Institute, Inc., Cary, NC).

Results

Polymeric Mesh Characterization

Electrospinning conditions were optimized to achieve fiber diameters which averaged 390 ±140 nm (*Nano-1*), 740 ± 160 nm (*Nano-2*), and 1420 ± 370 nm (*Micro*) for unaligned fiber matrices and 650 ± 170nm for the *aligned* matrix (Figure 1 and Table 1). Fiber diameters of the unaligned matrices were statistically different from each other ($p<0.05$). In contrast, no difference in fiber diameter was found between the *aligned* and *unaligned Nano-2* meshes.

Alignment analysis results [mean vector angle (MA), mean vector length (MVL) and angular deviation (AD)] are summarized in Table 1. While the MVL and AD of the *Nano-2* group differed from the other unaligned groups, overall the values for these parameters were

indicative of a disorganized fiber morphology. Analysis confirmed the organization of nanofibers in the *Nano-2* aligned group, and as expected, all unaligned groups were significantly different from the aligned group in MA, MVL and AD.

Effect of diameter on cell attachment and organization

Cells remained viable on all scaffolds tested over the four-week culture period. Focal adhesions (pink) and actin filaments (green) were visualized using immunohistochemistry. Cell adhesion and spreading were enhanced as fiber diameter increases (Figure 2). Cell polarization was evident after one hour of culture in the *Micro* group, while cells on nanofiber matrices still appeared rounded. Furthermore, after one day of culture, cells in the *Micro* group appeared more elongated and organized relative to the nanofiber scaffolds (*Nano-1* and *Nano-2)* despite the fact that all three substrates are unaligned.

Differences in cell alignment were also observed during the first two weeks of culture, and in general, cells became more organized over time. Specifically, at day 1, the MA of the *Nano-1* and *Nano-2* groups was significantly larger than the *Micro* group, with a lower MA indicative of an organized orientation. At days 7 and 14, cell alignment parameters for *Nano-2* (MA, AD) and *Nano-1* (MVL, AD) groups continued to indicate a greater degree of randomly oriented cells compared to the *Micro* group. Over time a significant increase in MVL and concurrent decrease in MA and AD were observed for all three unaligned groups, and by day 28 the only difference between groups was in AD between *Nano-1* and *Micro*.

Effect of fiber diameter on cell growth and phenotype

Fibroblasts proliferated in all groups through the four-week culture period. While a temporal increase in cell number was observed in all groups (Figure 3), at day 28, cell number on the nanofiber matrices were greater than that on the *Micro* group ($p<0.05$). Hematoxylin staining revealed that cell distribution was uniform through the depth of the scaffold for all groups.

A significant increase in collagen production over time was observed for the *Nano-1* and *Nano-2* groups (Figure 3). Furthermore at day 28, collagen per scaffold was significantly greater for the *Nano-2* group compared to the *Micro* group. Picrosirius red staining at day 28 (Figure 3) confirms the synthesis of a collagen-rich matrix. A more intense staining was observed in the *Nano-1* and *Nano-2* groups compared to the *Micro* group.

The expression of collagens I and III, and integrins α2 and β1 were examined at days 7 and 14. After one week of culture, an upregulation of collagens I and III was observed in the *Micro* group compared to both nanofiber matrices. There was a significant decrease in collagen I and III expression for both *Nano-1* and *Micro* groups over time. The ratio of collagen III/I expression increased over time for the *Nano-1* group. At day 7, the expression of α2 was significantly downregulated on the nanofiber matrices compared to the *Micro* group, while β1 expression was upregulated in *Nano-2* compared to *Nano-1*. The expression of integrins increased significantly from day 7 to 14 for all groups.

Effect of fiber alignment on cell attachment and organization

Cell adhesion was promoted in the *Aligned* group as indicated by more intense positive staining for paxillin (Figure 4). This is particularly evident at 30 minutes and 1 hour post-seeding. After 1 hour, an aligned actin fiber organization was evident on the aligned matrix. In contrast, no such organization of cell adhesions or actin fibers was noted for the unaligned *Nano-2* group.

Cell alignment analysis revealed a significantly larger MA and AD, and smaller MVL on unaligned fibers during the first two weeks of culture. With time, cells on the unaligned fibers became significantly more aligned, and by day 28, there were no significant differences in alignment parameters between the *Aligned* and unaligned *Nano-2* groups.

Effect of fiber alignment on cell growth and phenotype

Cell proliferation was noted over time (Figure 5) and at day 28, the cell number was significantly greater on the unaligned compared to the *Aligned Nano-2* mesh. Cell penetration, as observed with hematoxylin staining, was more extensive on unaligned fibers compared to aligned. Collagen deposition increased with culture time. Hematoxylin & Eosin as well as Picrosirius red staining at day 28 confirms a greater degree of matrix deposition on unaligned fibers.

At day 14, the expression of collagen III was significantly upregulated on unaligned nanofibers (Figure 5). Collagen I expression decreased over time for both groups, while collagen III decreased between day 7 and 14 for the aligned group.

Effect of fiber diameter and alignment on Rho GTPase expression and activity

After 1 day of culture, RhoA was upregulated on the *Nano-1* group compared to all other unaligned matrices ($p<0.05$), and Rac1 was upregulated on *Nano-1* compared to *Nano-2* ($p<0.05$), while no difference in neither Cdc42 expression nor Rac1 activity as a function of diameter was observed (Figure 6). Comparing results based on fiber alignment, Cdc42 was upregulated on aligned nanofibers, while active Rac1 was significantly lower than that of the unaligned *Nano-2* group.

Discussion

Models to study wound repair and healing are important for investigating the biology of tissue repair and regeneration, yielding critical insights that can guide the design and evaluation of therapies that will support and promote tissue regeneration. This study investigates the response of human tendon fibroblasts as a function of matrix fiber diameter and alignment, using PLGA fiber mesh models designed to represent the various stages of tendon repair post injury (Figure 1). PLGA is used as a prototypical polymer as it is a well-studied biodegradable material with highly tunable properties. Additionally, as the polymer degrades via bulk erosion, mesh fiber diameter and architecture are maintained, and mechanical properties remain within the range of the native tendon after four weeks of *in vitro* culture[8]. Observations from this study indicate that both matrix fiber diameter and alignment regulate fibroblast adhesion, spreading, and organization. In turn, downstream

response, including proliferation, gene expression, and matrix deposition are also modulated by these matrix parameters. A distinct cell response is observed with changes in model fiber diameter and alignment, with matrix alignment as an important design factor for biological healing of soft tissue injuries.

The unaligned mesh models used in this study are designed to simulate a wound environment, with a disorganized fiber matrix but increasing fiber diameter as wound healing progresses. It is observed here that culture on substrates mimetic of early injury states stimulates cells to proliferate and deposit matrix, which is characteristic of the initial fibroblast response displayed during wound healing[1]. In contrast, fibers with a larger, micron-sized, diameter, representing a more mature wound environment, promoted better cell organization, which in turn facilitates wound closure. Additionally, upregulation of integrin expression observed on the microfibers is suggestive of matrix remodeling or contraction[32], characteristic of the later stages of wound repair[3,4]. As such, these disorganized matrices fail to support the maintenance of the fibroblast phenotype and better represents the scar tissue. In contrast, an aligned morphology which more closely resemble the matrix of healthy tendons during development, inherently promotes cell organization, spreading, and maintenance of the fibroblastic phenotype.

At the cellular level, the results of this study are suggestive of the link between sub-cellular geometry and global cell function. Cells respond to their environment through cytoskeletal components that activate downstream signaling cascades[33]. The interactions between cells and their substrata are mediated by cytoskeletal components such as paxillin, an adapter protein which binds a variety of signaling molecules, and is localized to focal adhesions[34], and actin cytoskeletal fibers. Both focal adhesion formation as well as cytoskeletal organization is enhanced by culture on unaligned micron-sized fibers, where the tendon fibroblasts appear to be more elongated and organized relative to those on the unaligned nanofiber models. Moreover, paxillin is known to affect the activity of molecules such as the Rho family of GTPases[32,35], which in turn, control a variety of signal transducing pathways regulating responses such as cytoskeletal reorganization, transcription, and cell migration[36]. To further explore this expression of RhoA, Rac1, and, Cdc42, proteins from the Rho family of GTPases were evaluated. As GTPases alternate between active (GTP-bound) and inactive (GDP-bound) states, the amount of active Rac1 produced by the cells was also assessed. Critical to the tissue repair process is cell migration[32]. Rac and Cdc42 stimulate formation of lamellipodia and filopodia[37,38] respectively, at the front of migrating cells. Furthermore, Cdc42 mediates cell polarization, which is also required for movement[32,39]. Rho acts at the rear of the cells generating contractile forces[32,37], while also playing a role in maintaining cell adhesion[40]. Thus the cooperative action of these proteins promotes cell motility. Nur-E-Kamal *et al.* reported that unaligned Ultra-Web fibers with an average diameter of 180 nm promotes the activation of Rac over 2D substrates[41]. Jaiswal *et al.* observed that the fiber diameter of poly methyl methacrylate unaligned fibers can modulate the activation patterns mitogen-activated protein kinases (MAPKs)[42]. Results indicated that as fiber diameter decreases from 2.41 μm to 882 nm p38 activity increases, while a further decrease in diameter to 605 nm caused a decrease in activity. A similar but opposite trend was noted for p38 activity, highlight the varying effect that fiber diameter can have on cell phenotype response.

The observations of this study, where the expression of both RhoA and Rac1 are upregulated on the unaligned nanofibers, coupled with enhanced activity of Rac1 by fibroblasts on unaligned compared to aligned nanofibers, are indicative of enhanced cell motility on the unaligned nanofibers. As greater cell motility is commonly associated with wound contraction and tissue repair[32], cells on the unaligned nanofibers are likely progressing toward scar tissue formation rather than biological healing. Given that fiber diameter of the Nano-2 and Nano-2 aligned group are statistically similar, it is interesting that by altering fiber alignment, active Rac 1 level is reduced while the cells become more polarized, suggesting that fibroblast response on the nanofiber substrates maybe be changed from repair to healing by controlling matrix alignment.

Given that the organization of focal adhesions and actin fibers were enhanced on aligned fibers compared to unaligned immediately post seeding, it is not surprising that downstream cell responses are in turn affected, with both much lower cell growth and collagen deposition observed on aligned nanofibers, indicative of a normal healing response instead of the commonly observed proliferative phase of wound repair. The observed response of fibroblast on the aligned nanofiber also confirms the findings of Erisken *et al.*, which explored human tendon fibroblast response to aligned PLGA nanofibers and microfibers[16]. Interestingly, once alignment is maintained on the fiber mesh, increasing the fiber diameter from nano- to micron-size further reduces cell proliferation and biosynthesis, and most importantly, promotes the expression of fibroblastic markers such as tenomodulin[16]. Collectively, these observations suggest that compared to fiber diameter, fiber alignment is a critical early matrix characteristic essential in directing tendon fibroblasts towards a physiologically relevant adhesion and organization. Thereafter, any increase in matrix fiber diameter will promote the maintenance of the tendon fibroblast phenotype, with alignment and fiber diameter collectively driving the cells towards biological healing. These observations suggest that aligned nanofiber meshes rather than microfibers are an optimal matrix for tendon regeneration. Aligned nanofibers promote a balance between cell growth and biosynthesis required for the remodeling of a biodegradable polymer matrix, and the need to direct cell adhesion and organization early in the healing process. It is likely the neotissue with physiological alignment will mature and increase in fiber diameter, which will ensure the maintenance of the fibroblast phenotype and progress towards biological healing.

Collectively, the results of this study demonstrate the promise that synthetic fiber substrates have for modeling cell response to tendon injury and healing. While the unorganized fiber matrices of varied diameters can be used as a model of the different stages of tissue injury, aligned fibers can also be used to study regenerated or healthy tissue states. It is noted that the model systems presented here focus on fiber diameter and alignment. Many other factors can contribute to the complex cellular events and cell-matrix interactions which lead to scar-less healing. For example, the age of the patient that fibroblasts are harvested from can affect cell response to substrates. Specifically, no differences in cell proliferation were observed based on fiber alignment in a study which explored ACL fibroblast, which are typically harvested from younger patients, response to polyurethane fibers 500-800 nm[9] in diameter. Additionally, while an increase in col III/I ratio is often associated with scar tissue formation[43], it was observed here that the expression of col I and III were upregulated on the unaligned microfiber group, but there were no differences in col III/I ratio based on fiber

diameter. It is likely that other parameters, either matrix or cell-related, play a more important role in driving the collagen type ratio. Another limitation of these models is the lack of biological factors and immune cells typically involved in wound healing. As such, the relative simplicity of the fiber-based models allows the distillation of key matrix parameter, and their interplay in directing fibroblast response. Future studies will focus on enhancing the physiological relevance of the fiber-based model, further exploration of downstream effects as well as in vivo validation of these systems.

Conclusion

Modeling the events that occur during tissue repair and healing, this study explored the effect of fiber diameter of unaligned meshes and fiber organization on human tendon fibroblast response. The tissue repair model consisting of unaligned fibers with nanometer diameters promoted cell proliferation and matrix deposition synthesis as well as the expression and activity of RhoA and Rac1, characteristic of the initial, proliferative phase of wound repair. The mature repair model represented by unaligned micron-sized fibers supported cell organization and adhesion, while suppressing growth and biosynthesis, indicative of the remodeling phase of tissue repair. Finally, imparting alignment to nanofibers can guide cell response from repair to healing, potentially serving as a critical component to promoting the biological healing of soft tissues.

Acknowledgments

Funding Sources: This study was supported by NIH-NIAMS (5R01-AR055280, AR056459 HHL), a CTICE graduate research fellowship (NML).

References

1. Frank CB, Hart DA, Shrive NG. Molecular biology and biomechanics of normal and healing ligaments—a review. Osteoarthr Cartilage. 1999; 7(1):130–40.
2. Frank C, McDonald D, Bray D, Bray R, Rangayyan R, Chimich D, Shrive N. Collagen fibril diameters in the healing adult rabbit medial collateral ligament. Connect Tissue Res. 1992; 27(4): 251–63. PM:1576825. [PubMed: 1576825]
3. Frank C, McDonald D, Shrive N. Collagen fibril diameters in the rabbit medial collateral ligament scar: a longer term assessment. Connect Tissue Res. 1997; 36(3):261–9. PM:9512894. [PubMed: 9512894]
4. Doillon CJ, Dunn MG, Bender E, Silver FH. Collagen fiber formation in repair tissue: development of strength and toughness. Coll Relat Res. 1985; 5(6):481–92. PM:3833451. [PubMed: 3833451]
5. Lin TW, Cardenas L, Soslowsky LJ. Biomechanics of tendon injury and repair. J Biomech. 2004; 37(6):865–77. PM:15111074. [PubMed: 15111074]
6. Hildebrand KA, Frank CB. Scar formation and ligament healing. Can J Surg. 1998; 41(6):425. [PubMed: 9854530]
7. Gimbel JA, Van Kleunen JP, Mehta S, Perry SM, Williams GR, Soslowsky LJ. Supraspinatus tendon organizational and mechanical properties in a chronic rotator cuff tear animal model. J Biomech. 2004; 37(5):739–49. PM:15047003. [PubMed: 15047003]
8. Moffat KL, Kwei AS, Spalazzi JP, Doty SB, Levine WN, Lu HH. Novel nanofiber-based scaffold for rotator cuff repair and augmentation. Tissue Eng Pt A. 2009; 15(1):115–26. PM:18788982.
9. Lee CH, Shin HJ, Cho IH, Kang YM, Kim IA, Park KD, Shin JW. Nanofiber alignment and direction of mechanical strain affect the ECM production of human ACL fibroblast. Biomaterials. 2005; 26(11):1261–70. PM:15475056. [PubMed: 15475056]

10. Xie J, Li X, Lipner J, Manning CN, Schwartz AG, Thomopoulos S, Xia Y. “Aligned-to-random” nanofiber scaffolds for mimicking the structure of the tendon-to-bone insertion site. Nanoscale. 2010; 2(6):923–6. [PubMed: 20648290]
11. Meng ZX, Wang YS, Ma C, Zheng W, Li L, Zheng YF. Electrospinning of PLGA/gelatin randomly-oriented and aligned nanofibers as potential scaffold in tissue engineering. Mater Sci Eng C. 2010; 30(8):1204–10.
12. Subramony SD, Dargis BR, Castillo M, Azeloglu EU, Tracey MS, Su A, Lu HH. The guidance of stem cell differentiation by substrate alignment and mechanical stimulation. Biomaterials. 2013; 34(8):1942–53. PM:23245926 PMCID:3689925. [PubMed: 23245926]
13. Baker BM, Mauck RL. The effect of nanofiber alignment on the maturation of engineered meniscus constructs. Biomaterials. 2007; 28(11):1967–77. PM:17250888. [PubMed: 17250888]
14. Bashur CA, Dahlgren LA, Goldstein AS. Effect of fiber diameter and orientation on fibroblast morphology and proliferation on electrospun poly(D,L-lactic-co-glycolic acid) meshes. Biomaterials. 2006; 27(33):5681–8. PM:16914196. [PubMed: 16914196]
15. Bashur CA, Shaffer RD, Dahlgren LA, Guelcher SA, Goldstein AS. Effect of fiber diameter and alignment of electrospun polyurethane meshes on mesenchymal progenitor cells. Tissue Eng Pt A. 2009; 15(9):2435–45. PM:19292650.
16. Erisken C, Zhang X, Moffat KL, Levine WN, Lu HH. Scaffold fiber diameter regulates human tendon fibroblast growth and differentiation. Tissue Eng Pt A. 2013; 19(3-4):519–28. PM: 23150905.
17. Mathur A, Moore SW, Sheetz MP, Hone J. The role of feature curvature in contact guidance. Acta Biomater. 2012; 8(7):2595–601. PM:22426288. [PubMed: 22426288]
18. Giancotti FG. Integrin signaling: specificity and control of cell survival and cell cycle progression. Curr Opin Cell Biol. 1997; 9(5):691–700. [PubMed: 9330873]
19. Giancotti FG, Ruoslahti E. Integrin signaling. Science. 1999; 285(5430):1028–32. PM:10446041. [PubMed: 10446041]
20. Cary LA, Han DC, Guan JL. Integrin-mediated signal transduction pathways. Histol Histopathol. 1999; 14(3):1001–9. PM:10425567. [PubMed: 10425567]
21. Ozdemir T, Xu LC, Siedlecki C, Brown JL. Substrate curvature sensing through Myosin IIa upregulates early osteogenesis. Integrative Biology. 2013; 5(11):1407–16. [PubMed: 24104522]
22. Higgins AM, Banik BL, Brown JL. Geometry sensing through POR1 regulates Rac1 activity controlling early osteoblast differentiation in response to nanofiber diameter. Integrative Biology. 2015; 7(2):229–36. [PubMed: 25539497]
23. Grinnell F. Fibroblast biology in three-dimensional collagen matrices. Trends Cell Biol. 2003; 13(5):264–9. PM:12742170. [PubMed: 12742170]
24. Gurtner GC, Werner S, Barrandon Y, Longaker MT. Wound repair and regeneration. Nature. 2008; 453(7193):314–21. PM:18480812. [PubMed: 18480812]
25. Metcalfe AD, Ferguson MW. Tissue engineering of replacement skin: the crossroads of biomaterials, wound healing, embryonic development, stem cells and regeneration. J R Soc Interface. 2007; 4(14):413–37. PM:17251138. [PubMed: 17251138]
26. Gottrup F, Agren MS, Karlsmark T. Models for use in wound healing research: a survey focusing on in vitro and in vivo adult soft tissue. Wound Repair Regen. 2000; 8(2):83–96. PM:10810034. [PubMed: 10810034]
27. Costa KD, Lee EJ, Holmes JW. Creating alignment and anisotropy in engineered heart tissue: role of boundary conditions in a model three-dimensional culture system. Tissue Eng. 2003; 9(4):567–77. PM:13678436. [PubMed: 13678436]
28. Lu HH, Cooper JA Jr. Manuel S, Freeman JW, Attawia MA, Ko FK, Laurencin CT. Anterior cruciate ligament regeneration using braided biodegradable scaffolds: in vitro optimization studies. Biomaterials. 2005; 26(23):4805–16. PM:15763260. [PubMed: 15763260]
29. Pinnell SR. Regulation of collagen biosynthesis by ascorbic acid: a review. The Yale journal of biology and medicine. 1985; 58(6):553. [PubMed: 3008449]
30. Kim YJ, Sah RL, Doong JY, Grodzinsky AJ. Fluorometric assay of DNA in cartilage explants using Hoechst 33258. Anal Biochem. 1988; 174(1):168–76. PM:2464289. [PubMed: 2464289]

31. Wang IE, Mitroo S, Chen FH, Lu HH, Doty SB. Age-dependent changes in matrix composition and organization at the ligament-to-bone insertion. J Orthop Res. 2006; 24(8):1745–55. PM: 16779829. [PubMed: 16779829]
32. Ridley AJ, Schwartz MA, Burridge K, Firtel RA, Ginsberg MH, Borisy G, Parsons JT, Horwitz AR. Cell migration: integrating signals from front to back. Science. 2003; 302(5651):1704–9. PM: 14657486. [PubMed: 14657486]
33. Vogel V, Sheetz M. Local force and geometry sensing regulate cell functions. Nat Rev Mol Cell Biol. 2006; 7(4):265–75. PM:16607289. [PubMed: 16607289]
34. Cary LA, Guan JL. Focal adhesion kinase in integrin-mediated signaling. Front Biosci. 1999; 4:D102–D113. PM:9889179. [PubMed: 9889179]
35. Turner CE. Paxillin and focal adhesion signalling. Nature cell biology. 2000; 2(12):E231–E236. [PubMed: 11146675]
36. Etienne-Manneville S, Hall A. Rho GTPases in cell biology. Nature. 2002; 420(6916):629–35. PM: 12478284. [PubMed: 12478284]
37. Jaffe AB, Hall A. Rho GTPases: biochemistry and biology. Annu Rev Cell Dev Biol. 2005; 21:247–69. PM:16212495. [PubMed: 16212495]
38. Ridley AJ. Rho GTPases and cell migration. J Cell Sci. 2001; 114(Pt 15):2713–22. PM:11683406. [PubMed: 11683406]
39. Nobes CD, Hall A. Rho GTPases control polarity, protrusion, and adhesion during cell movement. J Cell Biol. 1999; 144(6):1235–44. PM:10087266. [PubMed: 10087266]
40. Ridley AJ, Hall A. The small GTP-binding protein rho regulates the assembly of focal adhesions and actin stress fibers in response to growth factors. Cell. 1992; 70(3):389–99. PM:1643657. [PubMed: 1643657]
41. Nur-E-Kamal, Ahmed I, Kamal J, Schindler M, Meiners S. Three dimensional nanofibrillar surfaces induce activation of Rac. Biochem Biophys Res Commun. 2005; 331(2):428–34. PM: 15850777. [PubMed: 15850777]
42. Jaiswal D, Brown JL. Nanofiber diameter-dependent MAPK activity in osteoblasts. J Biomed Mater Res A. 2012; 100(11):2921–8. PM:22700490. [PubMed: 22700490]
43. Vunjak-Novakovic G, Altman G, Horan R, Kaplan DL. Tissue engineering of ligaments. Annu Rev Biomed Eng. 2004; 6:131–56. PM:15255765. [PubMed: 15255765]

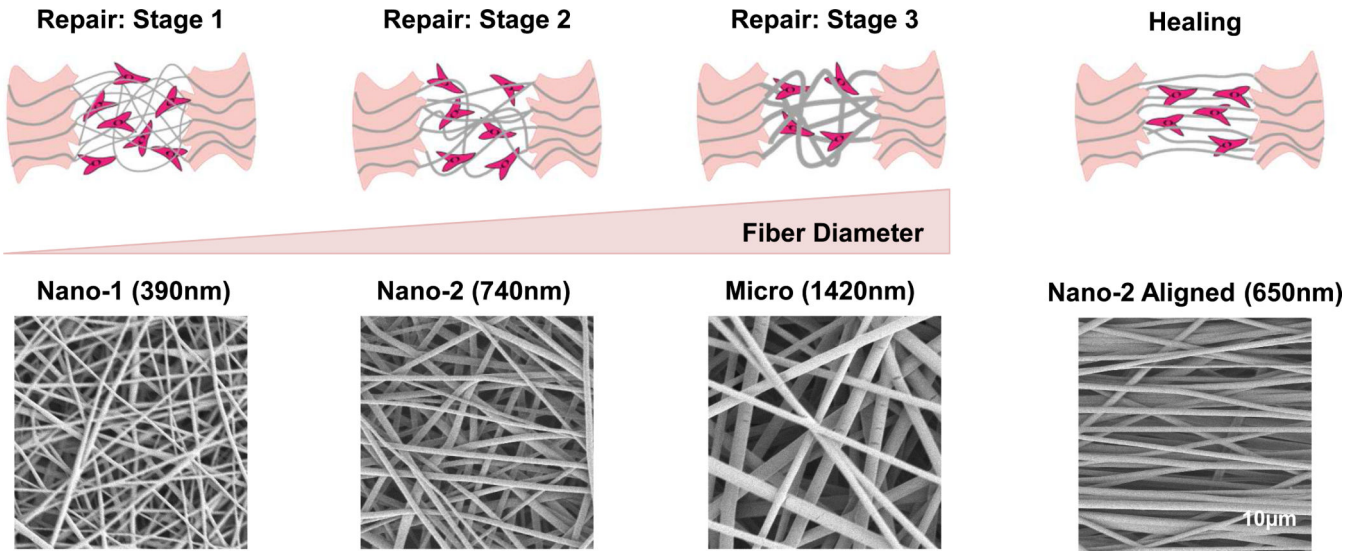

Figure 1.

The various stages of connective tissue repair are represented along with tissue healing are represented in the top panel. Scanning electron micrographs of the matrices used to model the corresponding stages of wound repair and healing are shown directly below.

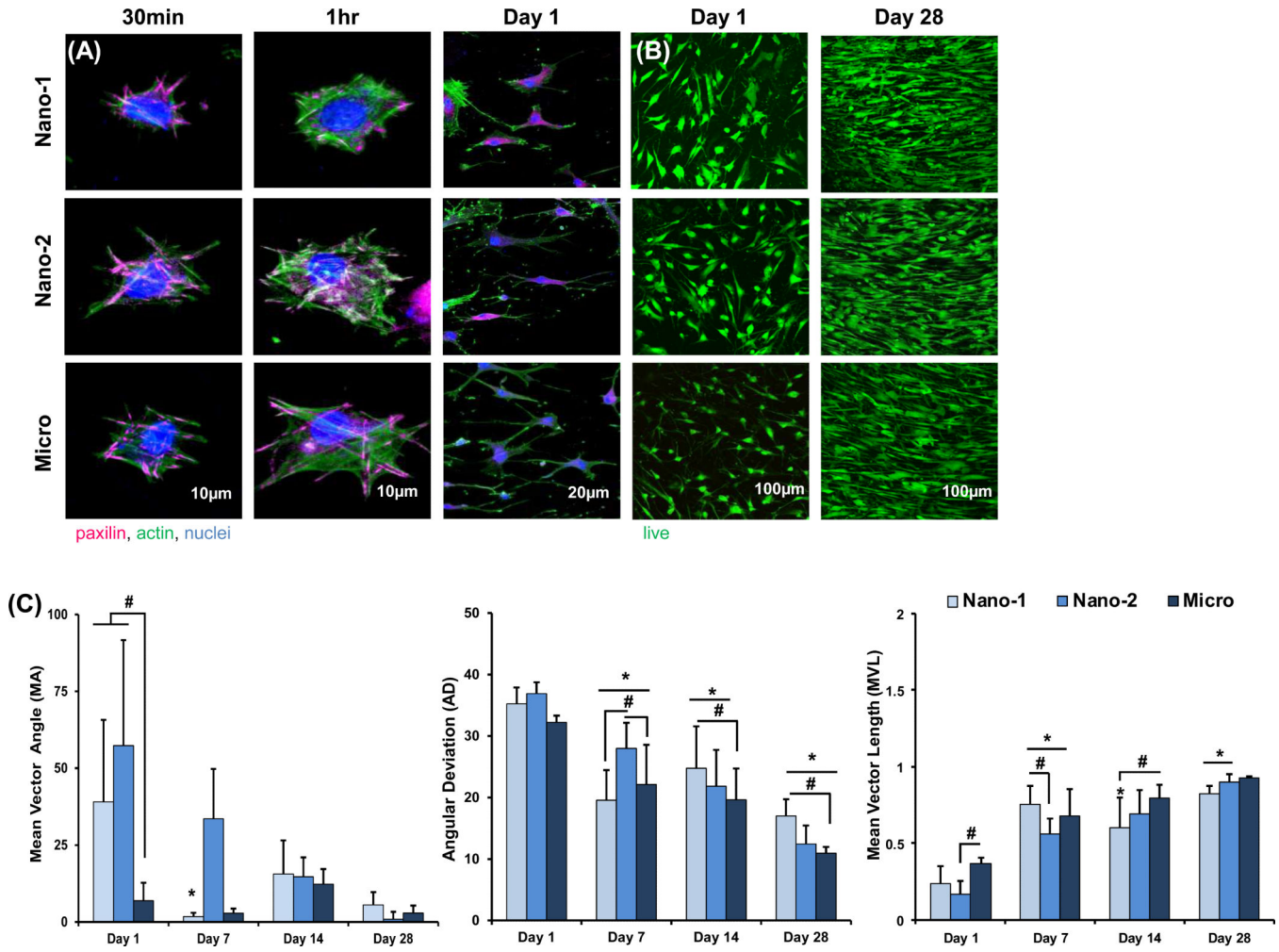

Figure 2. Effect of Fiber Diameter on Cell Attachment, Viability, and Alignment

(A) Immunohistochemistry was used to visualize cytoskeletal components at 30 minutes, 1 hour, and overnight, in which cell adhesions, spreading, and elongation increases with increasing fiber diameter and over time. (B) Cell viability is maintained and proliferation is noted on all groups. (C) Cell alignment is greatest on the Micro matrix during the first two weeks, and increases with time for all groups. Significant difference between: # groups, * consecutive timepoints ($n=5$, $p < 0.05$).

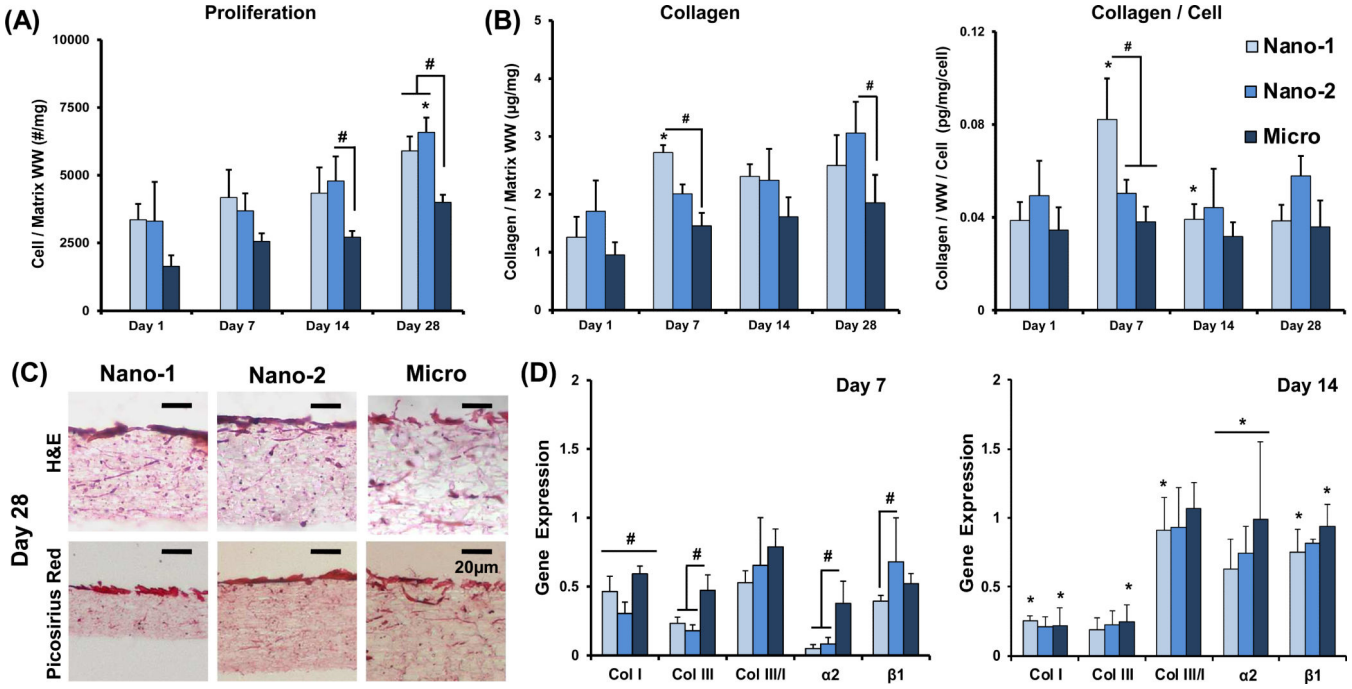

Figure 3. Effect of Fiber Diameter on Proliferation and Matrix Deposition

(A) Significant cell proliferation is noted for all groups over time (cell number/wet weight, n=5). (B) Collagen on nanofiber matrices is significantly greater compared to the Micro group (collagen/wet weight and collagen/wet weight/cell, n=5). (C) Collagen is deposited predominately at the substrate surface, with greater staining on Nano-1 and Nano-2 groups (H&E and picrosirius red, n=2). (D) The expression of col I and III, ratio col III/I, and integrins α2 and β1 were evaluated after 7 and 14 days of culture. Col I and III are upregulated on the Micro matrix compared to both Nano groups on day 7. The expression of collagens decreases over time. Integrin α2 is upregulated on Micro compared to both Nano groups at day 7, while β1 expression is upregulated on Nano-2 compared to Nano-1 (n=5). Significant difference between: # groups, * consecutive timepoints ($p < 0.05$).

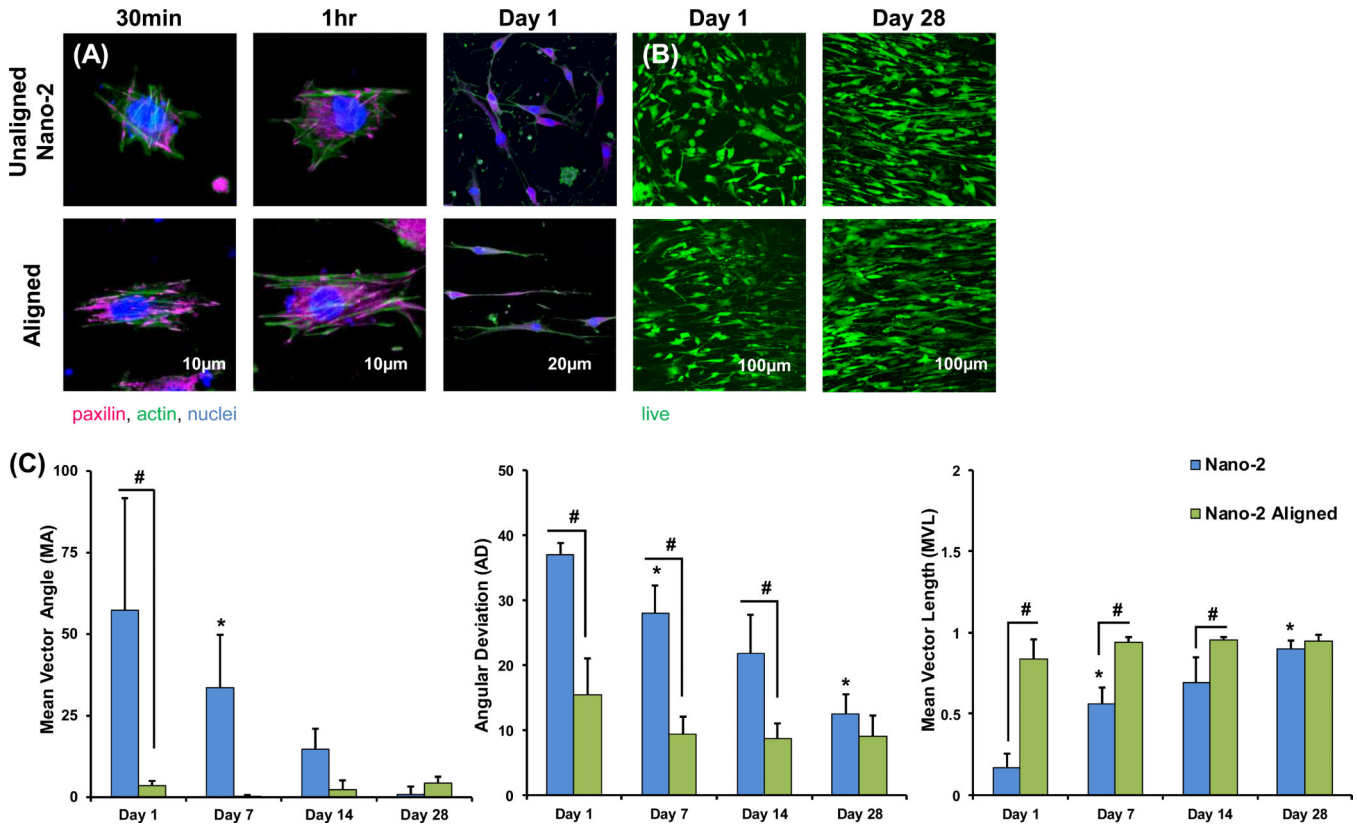

Figure 4. Effect of Fiber Alignment on Cell Attachment, Viability, and Alignment

(A) Immunohistochemistry was used to visualize cytoskeletal components at 30 minutes, 1 hour, and overnight, in which cell adhesions, spreading, and elongation is enhanced on aligned matrices at all timepoints. (B) Cell remain viable and proliferation is noted on both substrates. (C) Cells are significantly more organized on the aligned matrix (MA, MVL, AD) at Day 1, 7, 14, while cell alignment increases with time for the Nano-2, unaligned, group. Significant difference between: # groups, * consecutive timepoints ($n=5$, $p < 0.05$).

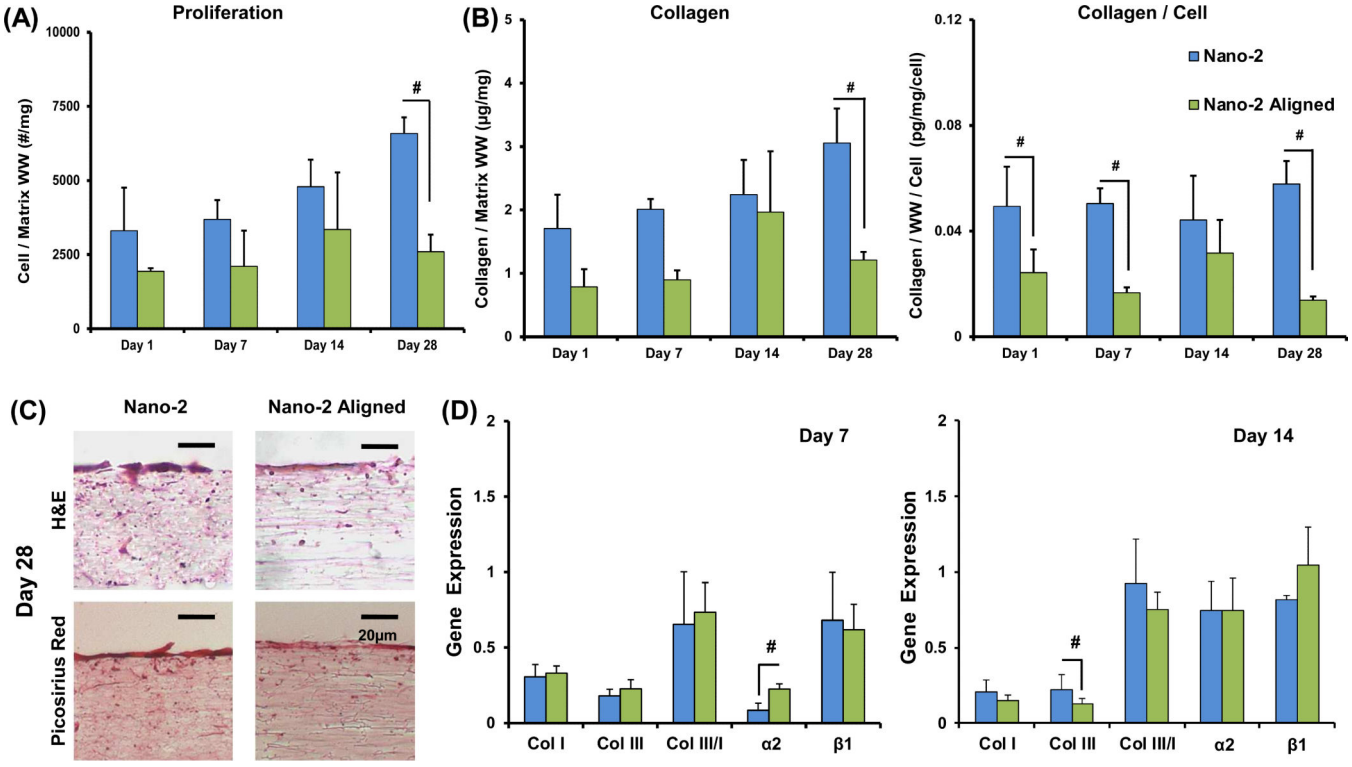

Figure 5. Effect of Fiber Alignment on Proliferation and Matrix Deposition

(A-B) Cell number and collagen is significantly greater on the unaligned matrices at Day 28 (cell number/wet weight, collagen/wet weight, collagen/wet weight/cell, n=5). (C) H&E histology shows greater cell penetration through the matrix depth on the unaligned group compared to the aligned (H&E and picrosirius red, n=2). (D) Gene expression of col I and III, ratio col III/I, and integrins α2 and β1 were evaluated after 7 and 14 days of culture. Integrin α2 expression is upregulated on the aligned matrix on day 7, and col III is upregulated on Nano-2 at day 14 (n=5). Significant difference between: # groups, * consecutive timepoints ($p < 0.05$).

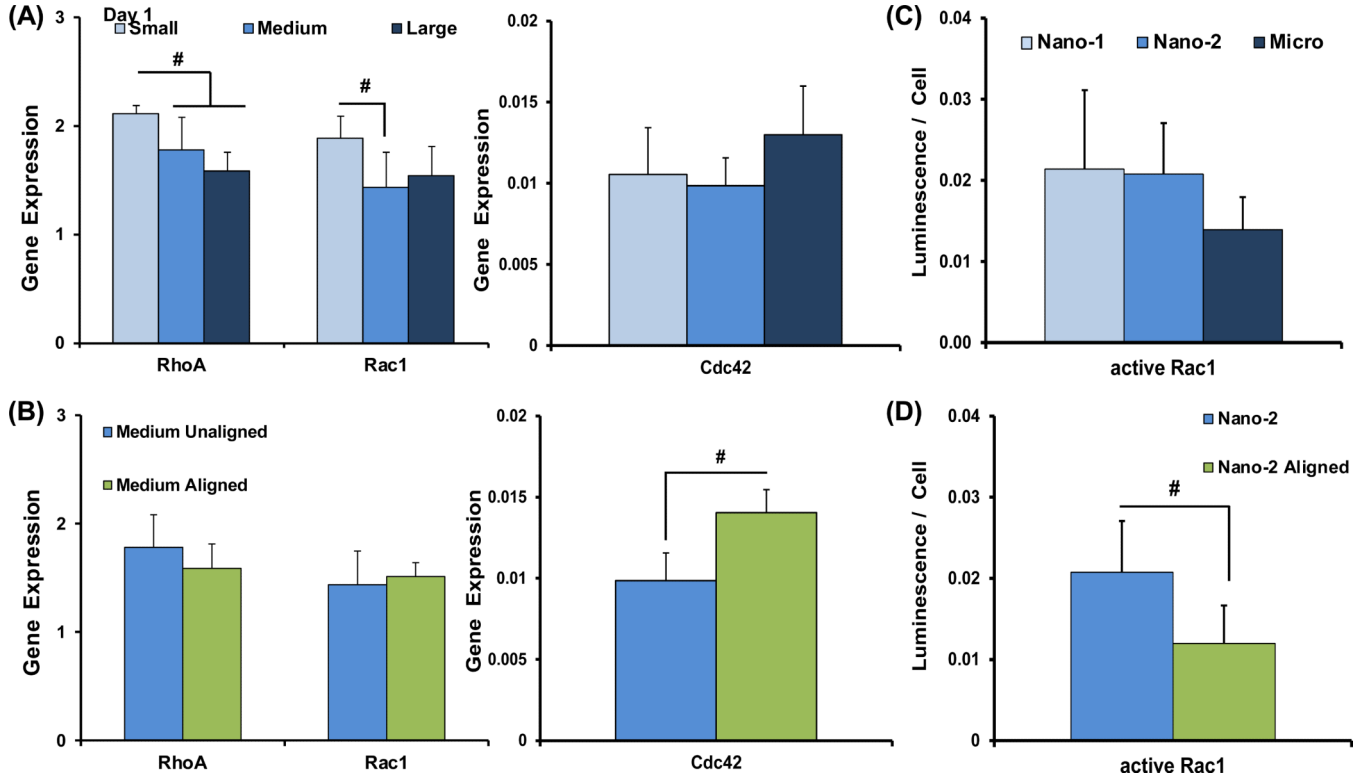

Figure 6. Rho GTPase Signaling Response to Matrices

The expression of RhoA, Rac1, and Cdc42 were evaluated at day 1, based on fiber diameter and alignment (n=5). (A) Evaluating the effects of fiber diameter, RhoA expression is upregulated on Nano-1 compared to all other groups and Rac1 expression is upregulated on Nano-1 compared to Nano-2. (B) Based on fiber alignment, Cdc42 is significantly upregulated on aligned matrices. (C-D) Active Rac1 was quantified after one day of culture (n=5). There were no differences based on fiber diameter, while significantly greater levels of active Rac1 was detected on the Nano-2 group compared to aligned. Significant difference between: # groups, * consecutive timepoints (n=5, $p < 0.05$).

Table 1

Electrospinning Conditions and Characterization of Fiber Alignment

Group	Fiber Diameter (nm)	Polymer (%wt/vol)	DMF:Ace	Flow Rate (ml/hr)	Needle Gauge	Mean Vector Angle (n=6)	Angular Deviation (n=6)	Mean Vector Length (n=6)
Nano-1	390 ± 140$^{\wedge}$	32%	70:30	0.35	26.5	49.55 ± 7.89^{A}	37.49 ± 0.50^{A,U}	0.14 ± 0.023^{A,U}
Nano-2	740 ± 160*	43%	80:20	0.35	26.5	48.39 ± 2.06^{A}	31.96 ± 1.04$^{\wedge}$	0.38 ± 0.040$^{\wedge}$
Micro	1420 ± 370$^{\wedge}$	50%	80:20	1	18	40.96 ± 16.80^{A}	37.97 ± 1.76^{A,U}	0.12 ± 0.08^{A,U}
Nano-2 Aligned	650 ± 170*	54%	100:0	1	18	0.53 ± 0.72$^{\wedge}$	8.54 ± 0.84$^{\wedge}$	0.96 ± 0.0089$^{\wedge}$

Fiber diameter values are an average of measurements taken from 3 independent regions imaged at 1 and 2.5K magnifications, with 20 measurements taken per image. No statistical differences in fiber diameter were noted between the Nano-2 (unaligned) and aligned groups. Alignment parameters of as-fabricated matrices are provided, in which a Mean Vector Angle of 0° indicates a horizontal orientation, an Angular Deviation of 0° is aligned and 40.5° is random, and Mean Vector Length of 1 is aligned and 0 is random.

Significant difference with:

^{A}aligned

^{U}Nano-2

*Nano-1 and Micro

$^{\wedge}$all groups (n=6, $p < 0.05$).

Table 2

Gene primer sequences for qRT-PCR

Gene	Sense	Antisense	Blast Product Size (bp)
GAPDH	5’-GGCGATGCTGGCGCTGAGTA-3’	5’-ATCCACAGTCTTCTGGGTGG-3’	306
Collagen I	5’-TGGTCCACTTGCTTGAAGAC-3’	5’-ACAGATTTGGGAAGGAGTGG-3’	118
Collagen III	5’-GGCTACTTCTCGCTCTGCTT-3’	5’-CATATTTGGCATGGTTCTGG-3’	130
α2	5’-CAGAATTTGGAACGGGACTT-3’	5’-CAGGTAGGTCTGCTGGTTCA-3’	333
β1	5’-GAGGAATACAGCCTGTGGGT-3’	5’-ATTGCAGGATTCAGGGTTTC-3’	121
RhoA	5’-GGGAGCTAGCCAAGATGAAG-3’	5’-GGTCTTTGCTGAACACTCCA-3’	55
Rac1	5’-CCATGGCTAAGGAGATTGGT-3’	5’-GTCTTGAGGCCTCGCTGT-3’	52
Cdc42	5’-TGGTGTCGGCATCATACTAAA-3	5’-TGTCTCACACGAGTGCATGT-3’	98